

Rare-Earth Nitrides and Carbides: A New Class of Permanent Magnet Materials

G.C. Hadjipanayis, Y.Z. Wang, E.W. Singleton, and W.B. Yelon

The most recent and exciting development in permanent magnet research is the discovery of rare-earth nitrides and carbides with the 2:17- and 1:12-type structures. Nitrogen and carbon enter the lattice interstitially, expanding the volume of the unit cell and leading to a drastic increase in the Curie temperature (up to 300 °C) and to dramatic changes in the magnetic anisotropy. $Sm_2Fe_{17}(N(C))_x$ and $Nd(Fe,T)_{12}N_x$ now have large magnetic anisotropy fields exceeding 9 and 7 T, respectively. Large coercivities have already been obtained in mechanically alloyed powders, melt-spun ribbons, and Zn-bonded $Sm_2Fe_{17}N_x$ magnets.

1 Introduction

It is well known that the Sm_2Fe_{17} compound has a planar anisotropy and therefore is unsuitable for use as a permanent magnet material. However, recently it has been reported that the introduction of interstitial carbon or nitrogen atoms into the 2:17 structure drastically changes the intrinsic magnetic properties of $R_2Fe_{17}C_x$[1-3]and $R_2Fe_{17}N_x$[4]compounds, where R is a rare-earth metal. The Sm_2Fe_{17}-carbides and nitrides exhibit a large uniaxial anisotropy, as well as a dramatic increase in Curie temperature, which makes them promising for permanent magnet development. Similar changes in the intrinsic magnetic properties of $RFe_{10}V_2$ and $RFe_{11}Ti$ have been reported with the uptake of nitrogen in the 1:12 lattice.[5] In this article, the authors review their research in this area over the last two years, with more emphasis given to the structural and magnetic properties of the 2:17 and 1:12 compounds.

2 Experimental

2.1 *Sample Preparation*

2.1.1 As-Cast $Sm_2Fe_{17}C_x$

Alloys with nominal composition $Sm_2Fe_{17}C_x$ with $0 \leq x \leq 1.5$ were prepared by arc-melting high-purity (99.9%) materials under argon gas. Vaporization losses of Sm were compensated through addition of excess Sm. The ingots were sealed in evacuated quartz tubes and heat-treated at temperatures close to 1050 °C for 3 days to produce the Sm_2Fe_{17} carbides.

2.1.2 Nitrogenation by the Gas-Phase Interstitial Modification Process

Alloys with composition $RFe_{10}V_2$, $RFe_{10}Mo_2$, $RFe_{11}Ti$ (R=Y, Nd, Sm, Gd, Dy, and Er) and R_2Fe_{17} (R=Nd, or Sm) were prepared by arc-melting using materials of 99.9% purity. After arc-melting, the alloys were homogenized by vacuum-annealing at temperatures between 800 and 1000 °C for 1 to 7 days. These single-phase alloys were pulverized to a particle size below <44 μm, and then they were heat-treated in a 99.9999% pu-

G.C. Hadjipanayis, Y.Z. Wang, and **E.W. Singleton,** Department of Physics and Astronomy, University of Delaware, Newark, Delaware; and **W.B. Yelon,** University of Missouri Research Reactor, Columbia, Missouri.

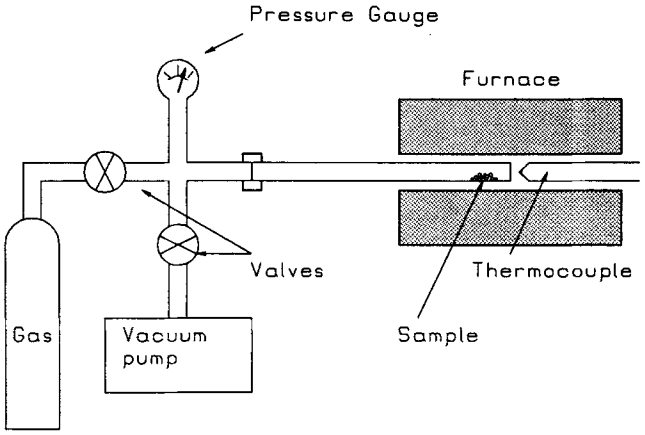

Fig. 1 Schematic layout of the apparatus used for the introduction of gas to the powdered sample.

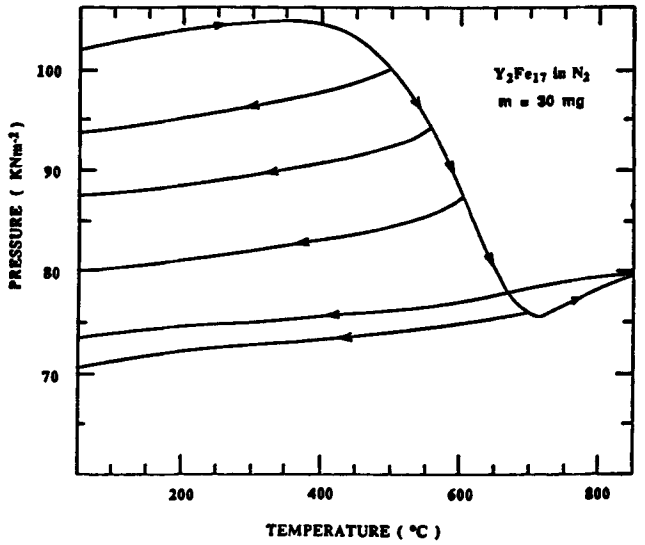

Fig. 2 Thermopiezic analyzer traces of Y_2Fe_{17} powders (Coey *et al.*[4]).

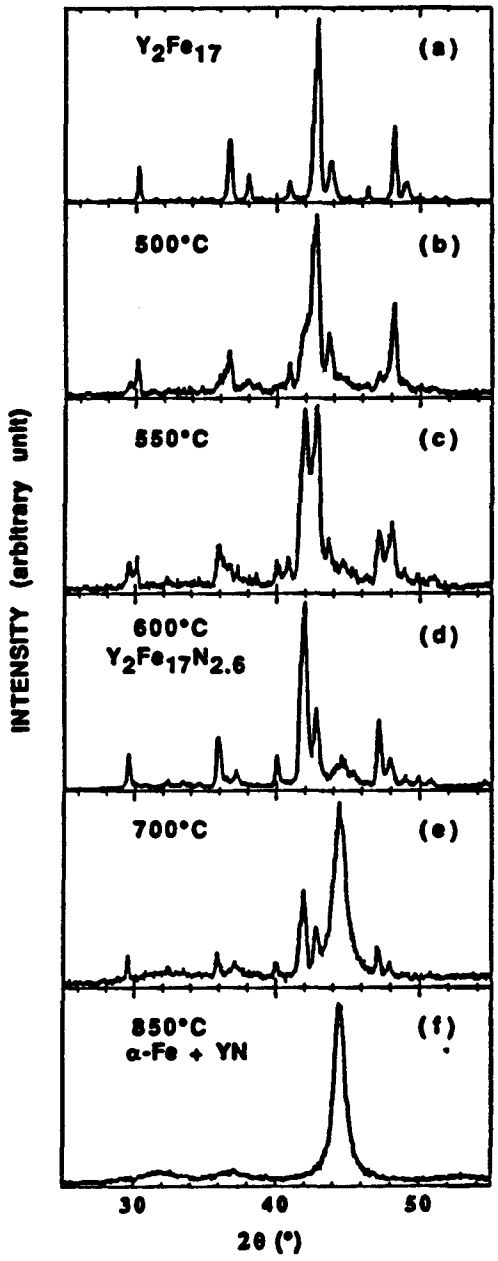

Fig. 3 X-ray diffraction patterns of Y_2Fe_{17} for increasing temperatures of nitrogen heat treatments (Coey *et al.*[4]).

rity nitrogen atmosphere for 1.5 to 3 hr at temperatures in the range of 500 to 600 °C. Figure 1 shows the apparatus used for the introduction of nitrogen gas to the powdered sample. Figures 2 and 3 show the results of one of the early experiments that led to the discovery of the nitrogenated rare-earth compounds. Coey and co-workers [6] monitored the change in nitrogen pressure by heat-treating Y_2Fe_{17} powders to temperatures in the range of 450 to 800 °C (Fig. 2) and the corresponding changes in the X-ray diffraction patterns (Fig. 3). At temperatures above 400 °C, N_2 pressure decreases, indicating that nitrogen is absorbed into the 2:17 lattice. This leads to an expansion of the unit cell and therefore a shift of the X-ray peaks to lower angles (Fig. 3). Complete absorption is made at around 600 °C. At higher temperatures, the sample is decomposed into α-Fe and YN.

2.2 *Sample Characterization*

X-ray diffraction patterns of the homogenized and nitrided powders were obtained using a Philips PW1710 diffractometer with a Cu-K_α radiation. The magnetic measurements at low temperatures were made with a SQUID magnetometer in magnetic fields up to 5.5 T and above room temperature with a vibrating sample magnetometer (VSM) in fields up to 1.7 T. Curie temperatures were determined using the VSM from thermal scans in a low magnetic field of 800 Oe. Neutron diffraction studies were made at the University of Missouri Research Reactor with $\lambda = 0.15472$ nm (1.5472 Å) using a position-sensitive detector.

3 Results and Discussion

3.1 *2:17 Nitrides*

Neutron diffraction studies[7] showed that nitrogen occupies the 9*e* sites of the rhombohedral Th_2Zn_{17}-type unit cell (Fig. 4) with $x = 2.8$. The interstitial nitrogen leads to an increase in both the lattice parameters *a* and *c*, with an approximate 6% increase in the unit cell volume (Fig. 5). Nitrogen atoms located very close to the R atoms strongly enhance the crystal-field-induced anisotropy of the rare-earth sublattice in $R_2Fe_{17}N_x$ compounds.[8,9] Indeed, X-ray diffraction and magnetic measurements performed on aligned powders confirm this assumption.[10] Figure 6 shows the X-ray diffraction pattern of the nitrided powders oriented in a magnetic field of 12 kOe compared with that of Sm_2Fe_{17} powders. It can be seen that the 006 reflection has the largest relative intensity and 220 and 300 are absent in $Sm_2Fe_{17}N_x$. The opposite behavior is found in Sm_2Fe_{17} and $Nd_2Fe_{17}N_x$, where the 006 reflection is absent and 220 dominates with 300. Such observation shows that the introduction of interstitial N atoms into the Sm_2Fe_{17} leads to an easy-axis anisotropy for $Sm_2Fe_{17}N_x$ compounds even at room temperature. However, $Nd_2Fe_{17}N_x$ still has an easy-plane anisotropy.

The X-ray diffraction results are consistent with the magnetization data parallel (M||) and perpendicular (M⊥) to the alignment direction at various temperatures, as shown in Fig. 7. Values of the magnetic anisotropy field (B_a) were obtained from intersections of the high field part of the M|| and M⊥ curves by extrapolation to high fields. It can be seen that the magnetic anisotropy field of $Sm_2Fe_{17}N_x$ at room temperature has a value around 9.5 T, which is higher than that of $Nd_2Fe_{14}B$. The saturation magnetization is also increased after nitrogenation, as shown in Fig. 8.[11]

Figure 9 shows the drastic change in the Curie temperature (T_c) of the 2:17 compounds upon nitrogenation. The highest T_c obtained in $Nd_2Fe_{17}N_x$ and $Sm_2Fe_{17}N_x$ compounds are 456 and 475 °C, respectively. These values are much higher than the 60 and 120 °C values measured on the original 2:17 compounds.

Attempts were made to obtain a high coercivity in $Sm_2Fe_{17}N_x$ powders by ball milling the nitrogenated powders

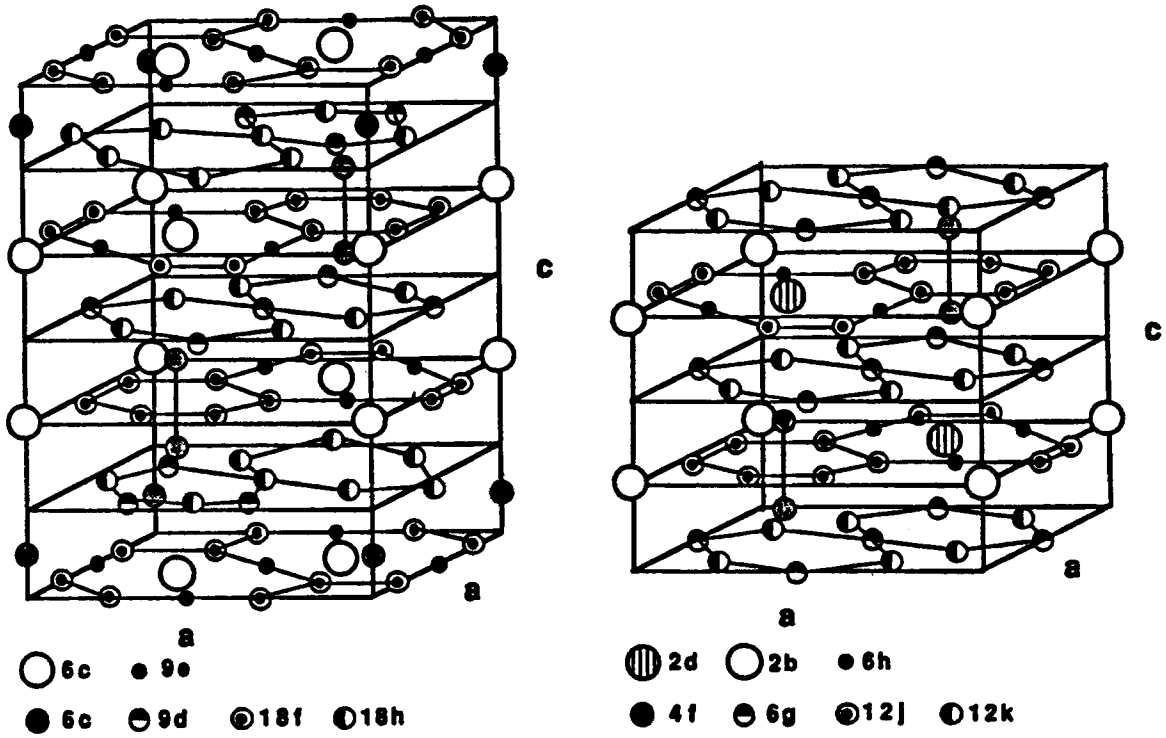

Fig. 4 Crystal structure of Th_2Zn_{17} (left) and Th_2Ni_{17} (right). The octahedral interstitial *9e* or 6h sites may be occupied by C or N.

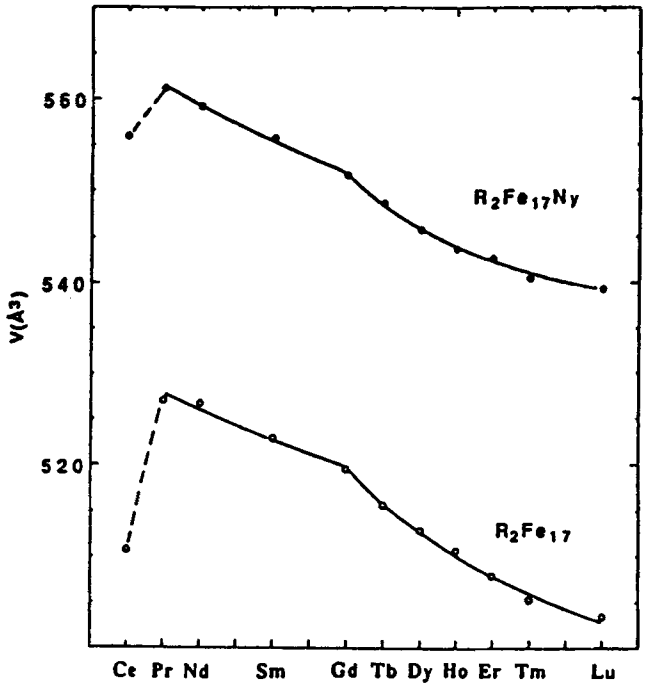

Fig. 5 Unit cell volume expansion for $R_2Fe_{17}N_x$ (Coey *et al.*[6]).

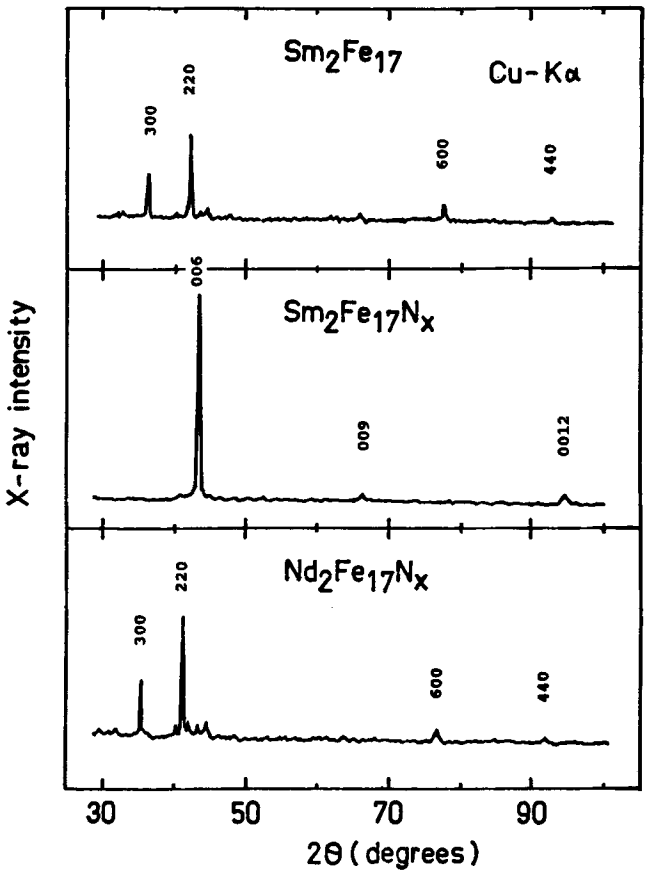

Fig. 6 X-ray diffraction patterns of aligned Sm_2Fe_{17}, $Sm_2Fe_{17}N_x$, and $Nd_2Fe_{17}N_x$ powders.

to a smaller particle size. Figure 10 shows a typical magnetic hysteresis loop for $Sm_2Fe_{17}N_x$ powders (6-μm size) at room temperature and at 10 K. The maximum coercivity obtained was only 6 kOe. However, the constricted shape of the hysteresis loop shows the presence of a phase with a much higher coer-

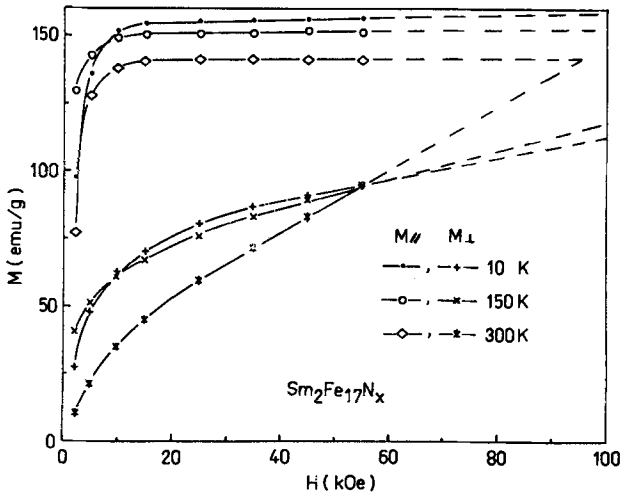

Fig. 7 Magnetization curves parallel and perpendicular to the alignment direction of $Sm_2Fe_{17}N_x$ at 10, 150, and 300 K.

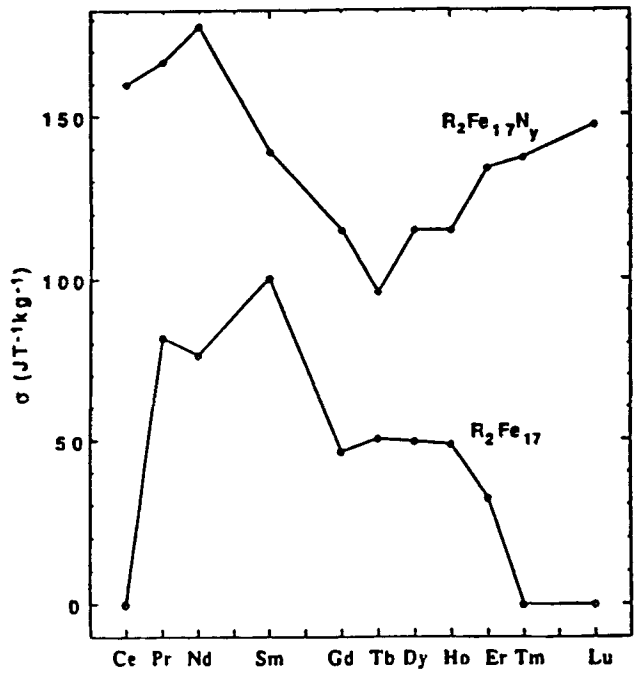

Fig. 8 Saturation magnetization for $R_2Fe_{17}N_x$ (Coey *et al.*[6]).

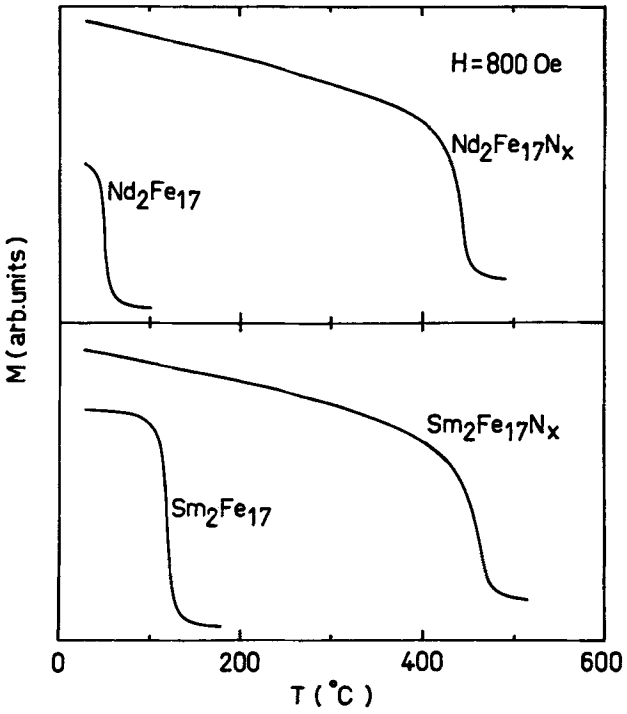

Fig. 9 Thermomagnetic scans for $Nd_2Fe_{17}N_x$ and $Sm_2Fe_{17}N_x$ along with the parent unnitrided compounds in an applied field of 800 Oe.

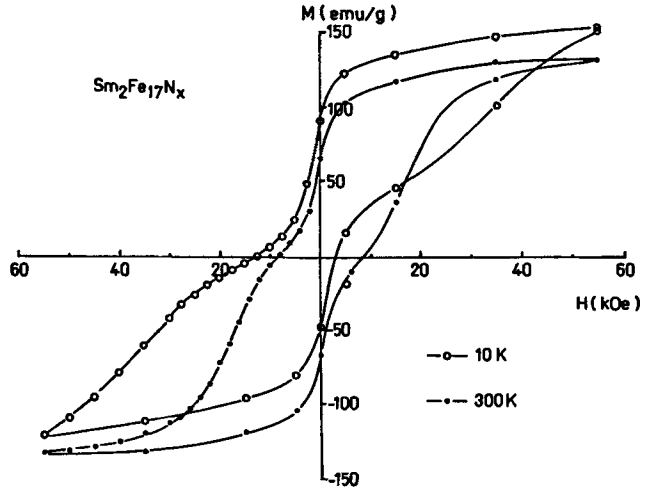

Fig. 10 Hysteresis loops of ball milled $Sm_2Fe_{17}N_x$ powders (6-μm size) at 10 and 300 K.

civity around 20 kOe (Fig. 10). This indicates that higher H_c can be achieved in these compounds that have a high anisotropy field. Indeed, very recently Schnitzke *et al.*[12] obtained an H_c = 30 kOe on mechanically alloyed $Sm_2Fe_{17}N_x$ alloys and Coey *et al.*[13] and Huang *et al.*[14] obtained coercivities exceeding 14 kOe in metal bonded magnets using a Zn-based matrix. The magnetic and structural properties of R_2Fe_{17} and $R_2Fe_{17}N_x$ compounds are summarized in Table 1 (Coey *et al.*[15]).

3.2 *2:17 Carbides*

X-ray powder analysis of the as-cast samples has shown that the single-phase $Sm_2Fe_{17}C_x$ compounds do not form directly from the melt. Usually, in addition to the 2:17:x phase with a Th_2Zn_{17}-type structure, the $SmFe_2$ phase and a small amount of α-Fe are observed in the as-cast samples. Single-phase 2:17:x can be formed by a suitable annealing at about 1050 °C. X-ray diffraction analysis has also shown that samples annealed at different times have different lattice parameters. Thermomagnetic analysis data also confirm these results (Fig. 11). The Curie temperature of the Sm-Fe-C compounds is much higher than that in Sm_2Fe_{17}(T_c ~ 130 °C),[16] but significantly lower than in $Sm_2Fe_{17}N_x$. From the thermomagnetic analysis data in $Sm_2Fe_{17}C_{0.25}$ at various annealing times, one can clearly see

Table 1 Structural and Magnetic Properties of R_2Fe_{17} and $R_2Fe_{17}N_x$

Alloy	Structure type	Lattice parameters, nm a	c	Curie temperature (T_c), K	σ_s, $JT^{-1}kg^{-1}$
Ce_2Fe_{17}	Th_2Zn_{17}	0.847	1.232	241	0
$Ce_2Fe_{17}N_{2.8}$	Th_2Zn_{17}	0.873	1.265	713	160
Pr_2Fe_{17}	Th_2Zn_{17}	0.857	1.242	290	82
$Pr_2Fe_{17}N_{2.5}$	Th_2Zn_{17}	0.877	1.264	728	167
Nd_2Fe_{17}	Th_2Zn_{17}	0.856	1.244	330	77
$Nd_2Fe_{17}N_{2.3}$	Th_2Zn_{17}	0.876	1.263	732	178
Sm_2Fe_{17}	Th_2Zn_{17}	0.854	1.243	389	100
$Sm_2Fe_{17}N_{2.3}$	Th_2Zn_{17}	0.873	1.264	749	139
Gd_2Fe_{17}	Th_2Zn_{17}	0.851	1.243	477	46
$Gd_2Fe_{17}N_{2.4}$	Th_2Zn_{17}	0.869	1.266	758	115
Tb_2Fe_{17}	Th_2Zn_{17}	0.845	1.241	404	51
$Tb_2Fe_{17}N_{2.8}$	Th_2Zn_{17}	0.866	1.266	733	96
Dy_2Fe_{17}	Th_2Ni_{17}	0.845	0.830	367	50
$Dy_2Fe_{17}N_{2.5}$	Th_2Ni_{17}	0.864	0.845	725	115
Ho_2Fe_{17}	Th_2Ni_{17}	0.844	0.828	327	49
$Ho_2Fe_{17}N_{3.0}$	Th_2Ni_{17}	0.862	0.845	709	115
Er_2Fe_{17}	Th_2Ni_{17}	0.842	0.827	296	32
$Er_2Fe_{17}N_{2.7}$	Th_2Ni_{17}	0.861	0.846	697	134
Tm_2Fe_{17}	Th_2Ni_{17}	0.840	0.828	260	0
$Tm_2Fe_{17}N_{2.7}$	Th_2Ni_{17}	0.858	0.847	690	137
Lu_2Fe_{17}	Th_2Ni_{17}	0.839	0.826	255	0
$Lu_2Fe_{17}N_{2.7}$	Th_2Ni_{17}	0.857	0.848	678	147
Y_2Fe_{17}	Th_2Ni_{17}	0.848	0.826	325	92
$Y_2Fe_{17}N_{2.6}$	Th_2Ni_{17}	0.865	0.844	694	164

Source: From Ref 15.

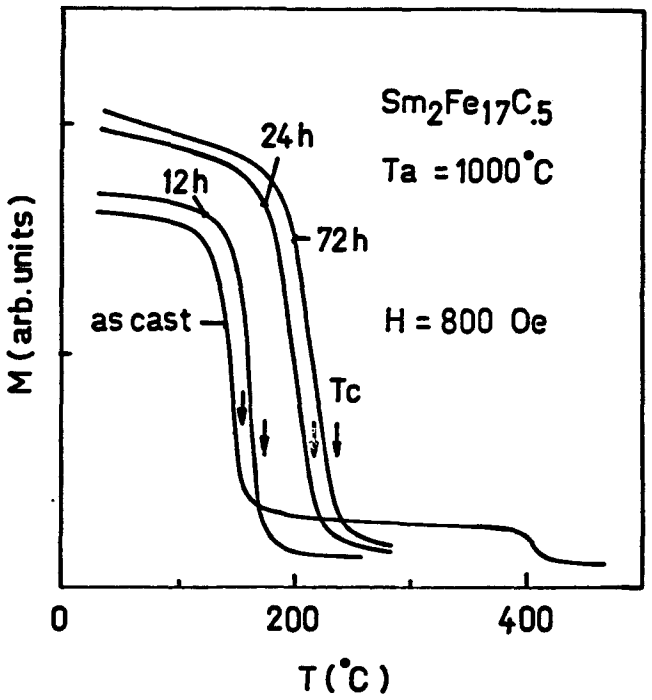

Fig. 11 Thermomagnetic analysis of $Sm_2Fe_{17}C_{0.5}$ for several annealing times.

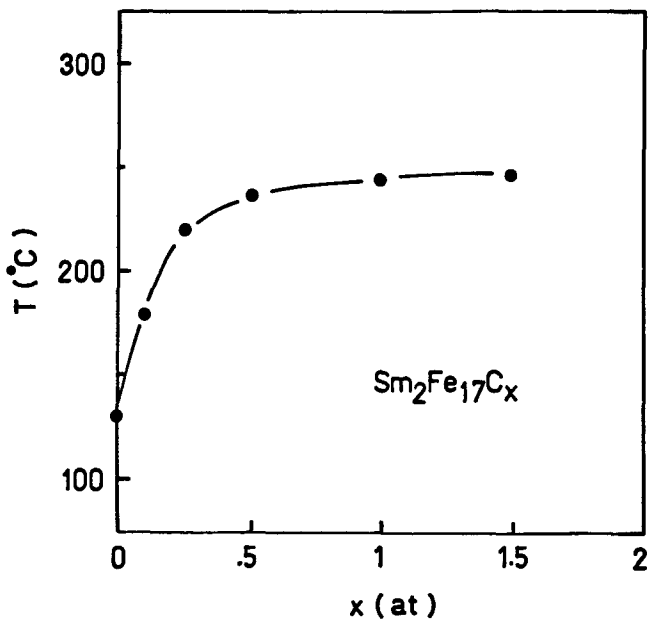

Fig. 12 Curie temperature as a function of carbon context (x) in $Sm_2Fe_{17}C_x$.

that the Curie temperature of the carbide is continuously shifted toward high temperatures with increasing annealing time. The dependence of Curie temperature on carbon content is very similar to that of the unit cell volume and is shown in Fig. 12.

The saturated values of lattice parameters and T_c indicate that the maximum amount of interstitial carbon obtained in heat-treated cast samples is only 0.5 as compared to 2.8 for nitrogen.

It is clearly seen from Fig. 13 that $Sm_2Fe_{17}C_{0.25}$ is characterized by an easy-axis anisotropy. Magnetocrystalline anisotropy constants were estimated from the magnetization curves obtained perpendicular to the alignment direction by a modi-

fied Sucksmith-Thomson technique, which was proposed by Ram and Gaunt.[17] The K_1 values at room temperature for various carbon concentration in $Sm_2Fe_{17}C_x$ are shown as a function of the carbon concentration in Fig. 14. The K_1 value is increasing with increasing x, and a transition from an easy-plane anisotropy to an easy-axis anisotropy takes place at about $x = 0.1$.

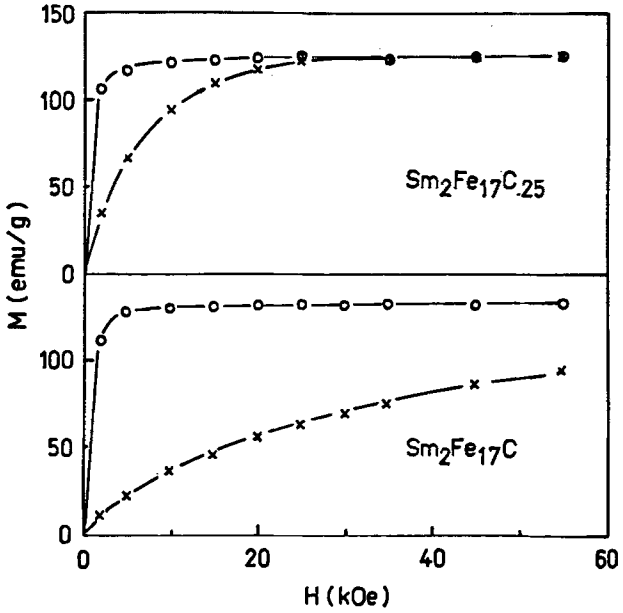

Fig. 13 Magnetization curves parallel (open circles) and perpendicular (x) to the alignment direction for $Sm_2Fe_{17}C_{0.25}$ and $Sm_2Fe_{17}C$ at room temperature.

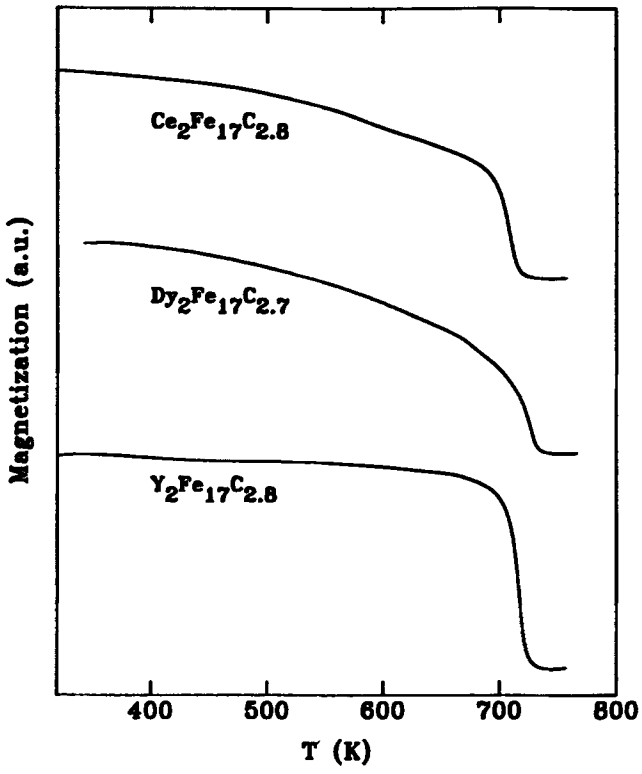

Fig. 15 Thermomagnetic scans for $R_2Fe_{17}C_x$, where R = Ce, Dy, or Y (Liao *et al.*, 1992).

Recently, Liao *et al.*[18] and Coey *et al.*[20] have successfully introduced larger amounts of carbon ($x \sim 2.8$) in the 2:17 parent alloy by performing gas-phase interstitial modification with hydrocarbon gas (methane, acetylene, or butane) at around 550 °C. The unit cell volumes and Curie temperatures (Fig. 15) found are comparable to those of the corresponding nitrides, and they are much larger than the values found in carbides obtained from the melt.

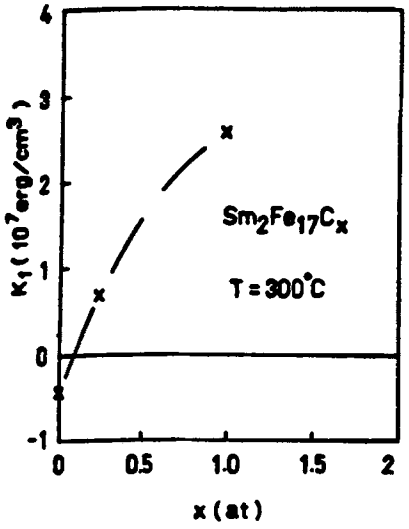

Fig. 14 Concentration dependence of the anisotropy constant K_1 in $Sm_2Fe_{17}C_x$.

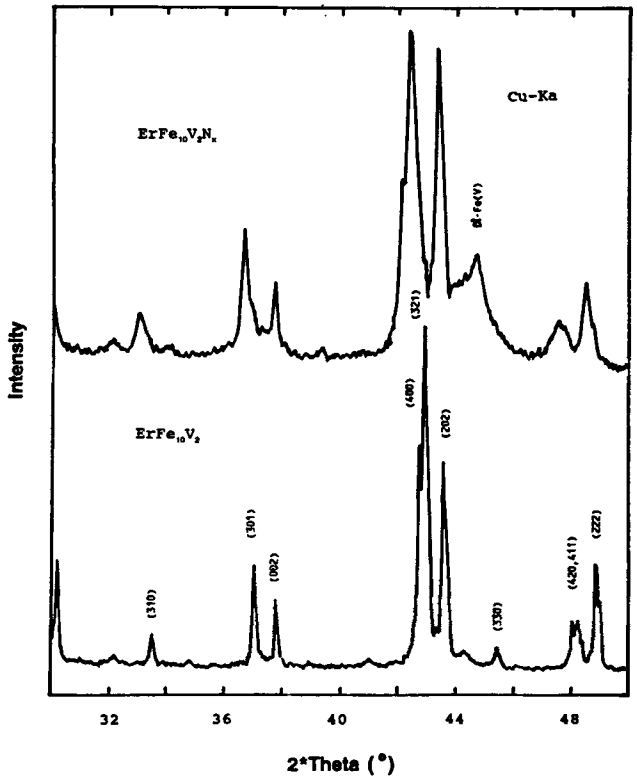

Fig. 16 X-ray diffraction patterns of $ErFe_{10}V_2$ and $ErFe_{10}V_2N_x$.

3.3 *$ThMn_{12}$-Type Structure Compounds (1:12)*

The Sm-containing compounds of the 1:12 type structure are found to be uniaxial, and coercivities in the 10-kOe range have been achieved in melt-spun ribbon samples[20] and in mechanically alloyed materials.[21] However, the 1:12 compounds still remain unattractive for permanent magnet development due to their relatively low magnetization and thus low $(BH)_{max}$ and because Sm is less abundant and therefore more expensive than Nd.

Effects of nitrogen uptake on the structural and magnetic properties of $RFe_{12-y}T_y$ (T = Mo, Ti, or V) alloys have yielded somewhat promising results. Several interstitial nitrides with the composition $RFe_{12-y}T_yN_x$ have been studied, which may lead to the eventual development of permanent magnets based on the 1:12 type alloys.

The X-ray diffraction patterns of $ErFe_{10}V_2$ before and after nitrogenation are shown in Fig. 16. Before nitrogenation, all alloys were almost composed of the 1:12 phase. However, after nitrogenation, there is a considerable amount of α-Fe(Ti) and α-Fe(V) phases in the $RFe_{11}TiN_x$ or $RFe_{10}V_2N_x$ samples with a broad peak at 2θ = 44.4°. The X-ray diffraction spectra of $RFe_{11}TiN_x$ and $RFe_{10}V_2N_x$ nitrides (R = Nd and Sm) were indexed in accordance with the tetragonal $ThMn_{12}$ structure. The lattice constants of these nitrides derived from X-ray diffraction are listed in Table 2, where they are compared with those of the original compounds. As seen in Table 2, the lattice constants, *a* and *c*, increase prominently due to the introduction of nitrogen into the 1:12 structure. The relative volume increase was found to be nearly constant, 2.5% ± 0.3.

Neutron diffraction data obtained on $NdFe_{10}Mo_2N_x$ powders were refined in the tetragonal space group *I4/mmm* with two formula units in the unit cell. The lattice parameters were found to be *a* = 0.86593(5) nm [8.6593(5) Å] and *c* = 0.48295(4) nm [4.8295(4) Å]. Nitrogen was found at the interstitial site of 001/2 (≡ 1/2 1/2 0), but with an occupancy of only ~ 1/2, indicating that only one of the two available sites per unit cell is filled. This site is the largest interstitial in the compound, and refinement for *N* occupancy of other sites failed to give val-

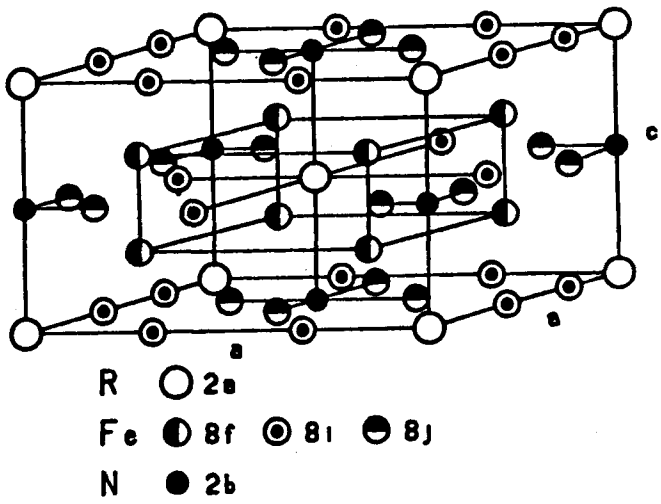

Fig. 17 Crystal structure for $RFe_{10}Mo_2N_x$ (tetragonal).

Table 2 Lattice Parameters, Unit Cell Volume, and Relative Volumes, for $RFe_{10}V_2N_x$ Compounds

$RFe_{10}V_2N_x$	Lattice parameters, nm		Unit cell volume (*V*), nm^3	Relative volumes (ΔV/V_0), %
	a	*c*		
R = Y	0.8592	0.4801	0.3544	3.0
	(0.8494)	(0.4770)	(0.3440)	
Nd	0.8624	0.4819	0.3584	2.4
	(0.8562)	(0.4775)	(0.3500)	
Sm	0.8613	0.4804	0.3563	2.5
	(0.8537)	(0.4772)	(0.3478)	
Gd	0.8574	0.4800	0.3529	2.7
	(0.8483)	(0.4776)	(0.3437)	
Dy	0.8579	0.4790	0.3525	2.9
	(0.8482)	(0.4760)	(0.3425)	
Er	0.8568	0.4776	0.3506	2.8
	(0.8471)	(0.4765)	(0.3419)	

Note: The data in parentheses pertain to the unnitrided materials.

Table 3 Refined Coordinates for $NdFe_{10}Mo_2N_x$ from Neutron Diffraction Data

		Coordinates		
	n	*x*	*y*	*z*
Nd	2	0	0	0
Fe	8	0.2753(5)	1/2	0
Fe/Mo	8	0.3607(5)	0	0
Fe	8	1/4	1/4	1/4
N	0.98(6)	0	0	1/2

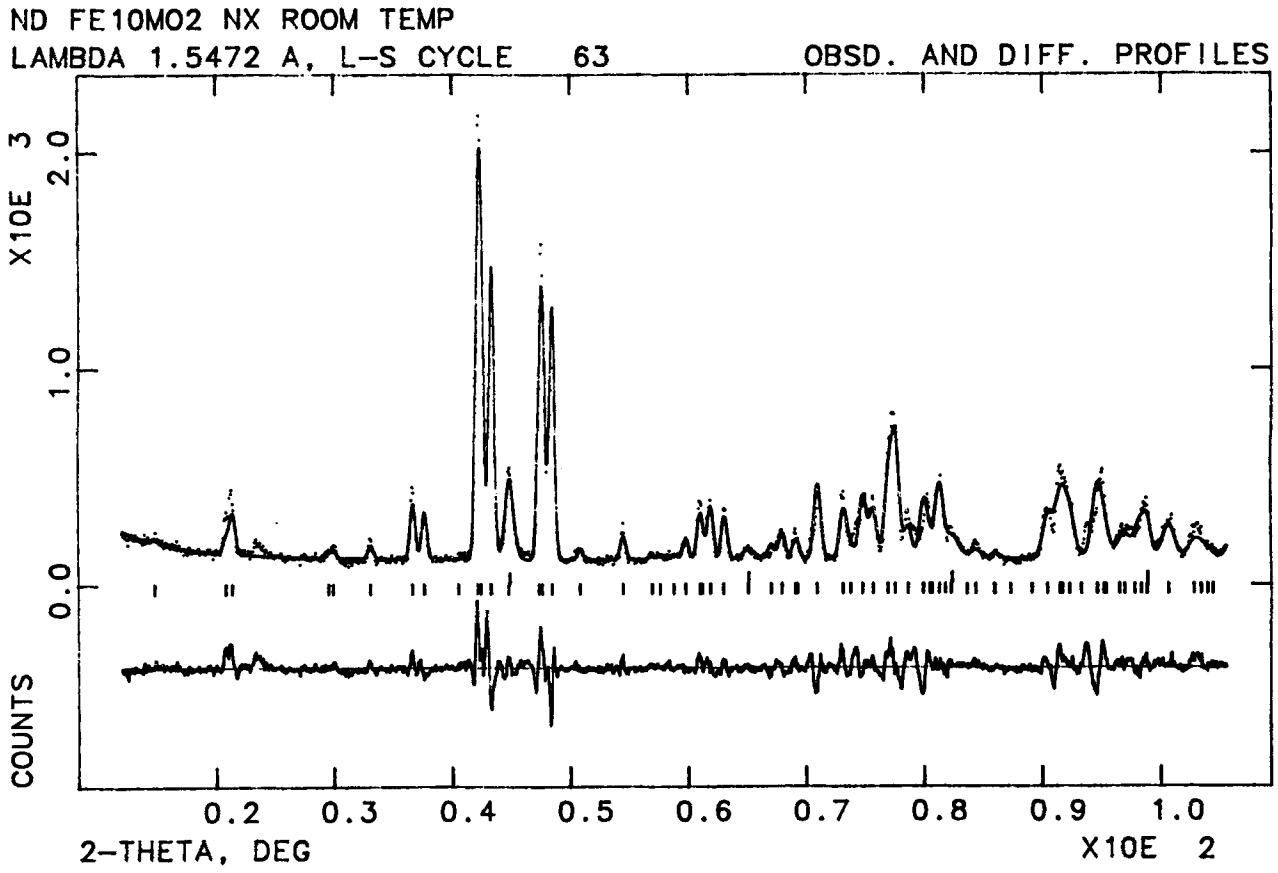

Fig. 18 Observed and difference profiles for $NdFe_{10}Mo_2N_x$ at room temperature.

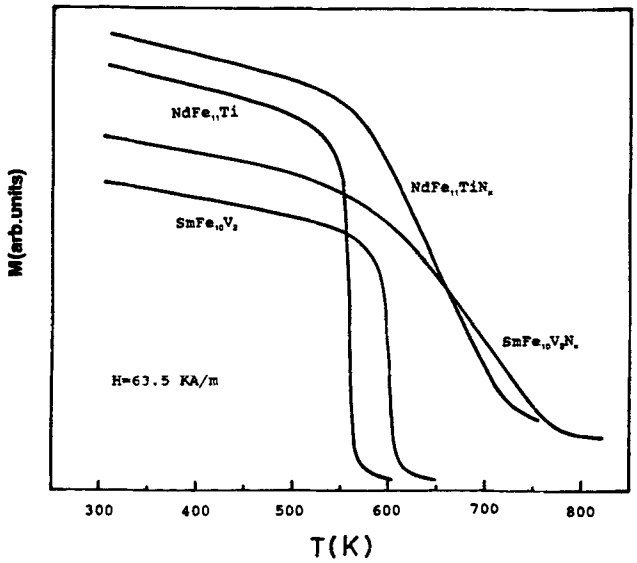

Fig. 19 Thermomagnetic data for $NdFe_{11}Ti$ and $SmFe_{10}V_2$ before and after nitrogenation.

ues statistically above zero. They are thus assumed to be vacant. The Mo atoms are found only on the transition metal site x,0,0 (x = 0.36) and replace 1/2 of the Fe on that site. Table 3 gives the refined coordinates (Fig. 17). In addition to the primary RTM_{12} phase, the refinement included a secondary (~ 6%) containment of α-Fe, which is indicated in the plot of the observed and difference diagrams (Fig. 18). The peaks were found to be significantly broadened compared to the instrumental resolution due to particle size and strain effects. Further analysis is underway to analyze the magnetic scattering.

Figure 19 shows the thermomagnetic data before and after nitrogenation for the $NdFe_{11}Ti$ and $SmFe_{10}V_2$ samples, respectively. It is clear that the nitrogen uptake enhances the Curie temperature of the nitrides remarkably. In addition, considerable amounts of α-Fe(Ti) (or α-Fe(V)) phases are formed with higher Curie temperatures, as indicated by the tailing off of the thermomagnetic curves shown in Fig. 19 (consistent with the X-ray diffraction results). The Curie temperatures and other magnetic properties of the nitrides are listed in Table 4, with those of the unnitrided materials shown in parentheses. The magnetic anisotropy field, B_a, was obtained from the magnetization curves measured parallel (M‖) and perpendicular (M⊥) to the aligning direction. The corresponding values of B_a are included in Table 4. The authors found that the nitrogen uptake changes the magnetic anisotropy of 1:12 structure substantially. When R = Nd, the $NdFe_{11}TiN_x$ and $NdFe_{10}V_2N_x$ compounds have a strong uniaxial anisotropy. Figure 20 shows the

Table 4 Curie Temperature, Saturation Magnetization, Easy Magnetization Direction, and Anisotropy Field in $RFe_{10}F_2N_x$

$RFe_{10}V_2N_x$	Curie temperature (T_c) K	Saturation magnetization (M_s), 10 K, ì B/formula unit	300 K, ì B/formula unit	Anisotropy field (Ba), 10 K, T	300 K, T	Easy magnetization direction at: 10 K	300 K
R = Y	767	19.4	16.4	3.8	1.9	*c*-axis	*c*-axis
	(537)	(16.2)	(14.0)	(4.8)	(2.7)	*c*-axis	*c*-axis
Nd	743	16.9	16.6	13.0	7.5	*c*-axis	*c*-axis
	(583)	(18.0)	(16.1)	...	(1.8)	Cone	*c*-axis
Sm	780	15.7	14.3	...	...	*ab*-plane	*ab*-plane
	(615)	(13.2)	(12.5)	(15.0)	(10.5)	*c*-axis	*c*-axis
Gd	795	11.5	11.2	...	...	*c*-axis	*c*-axis
	(610)	(8.9)	(8.9)	...	...	*c*-axis	*c*-axis
Dy	776	10.1	11.3	15.8	9.2	*c*-axis	*c*-axis
	(532)	(6.8)	(8.6)	(12.5)	(7.0)	Cone	*c*-axis
Er	730	9.3	13.4	...	2.5	*c*-axis	*c*-axis
	(507)	(8.4)	(12.8)	...	(3.3)	*ab*-plane	*c*-axis

Note: The data in parentheses pertain to the unnitrided materials.

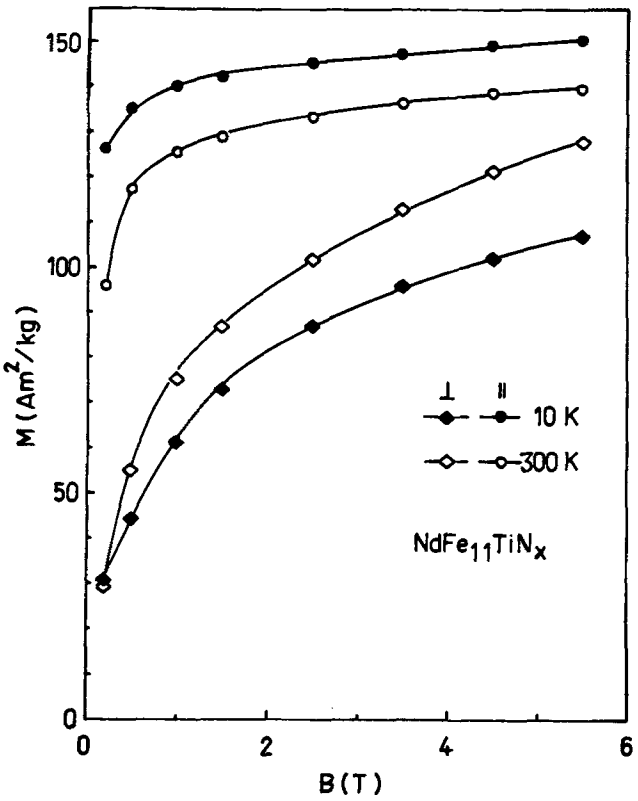

Fig. 20 Magnetization curves for oriented $NdFe_{11}TiN_x$ powder samples obtained parallel and perpendicular to the alignment field at 10 and 300 K.

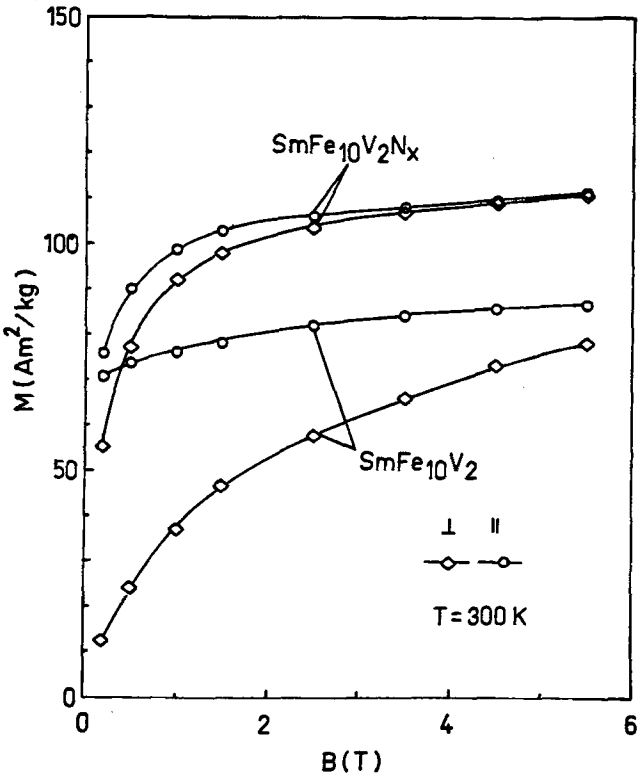

Fig. 21 Magnetization curves for oriented $SmFe_{10}V_2N_x$ powder samples obtained parallel and perpendicular to the alignment field.

magnetization curves of aligned $NdFe_{11}TiN_x$ powders at 10 and 300 K. The anisotropy field of $NdFe_{11}TiN_y$ increases to 9.5 T compared to the anisotropy field of $NdFe_{11}Ti$, which is only 2.4 T. This is attributed to an increase in the uniaxial magnetocrystalline anisotropy. For $NdFe_{10}V_2N_x$, the results are similar. On the contrary, when R = Sm, the magnetic anisotropy of the corresponding nitrides is decreased. Figure 21 shows the magnetization curves for $SmFe_{10}V_2$ and $SmFe_{10}V_2N_x$ at 300 K. It is known that $SmFe_{10}V_2$ has a large magnetic anisotropy field above 10.5 T, but for $SmFe_{10}V_2N_x$, M(||) and M(⊥) are very close together. The type of magnetic anisotropy of the nitrides was determined from X-ray diffraction patterns obtained on oriented nitride powders. Figure 22 shows a comparison of the X-ray diffraction patterns for oriented $SmFe_{11}TiN_x$ and $SmFe_{10}V_2N_x$ powders, with those of $SmFe_{11}Ti$ and $SmFe_{10}V_2$. It can be seen that the (002) reflection has the largest relative intensity on $SmFe_{11}TiN_x$ and $SmFe_{10}V_2N_x$. This indicates that the $SmFe_{11}Ti$ and $SmFe_{10}V_2$ compounds have a strong unaxial anisotropy. However, the behavior in $SmFe_{11}TiN_x$ and $SmFe_{10}V_2N_x$ is opposite, with the (002) reflection absent and

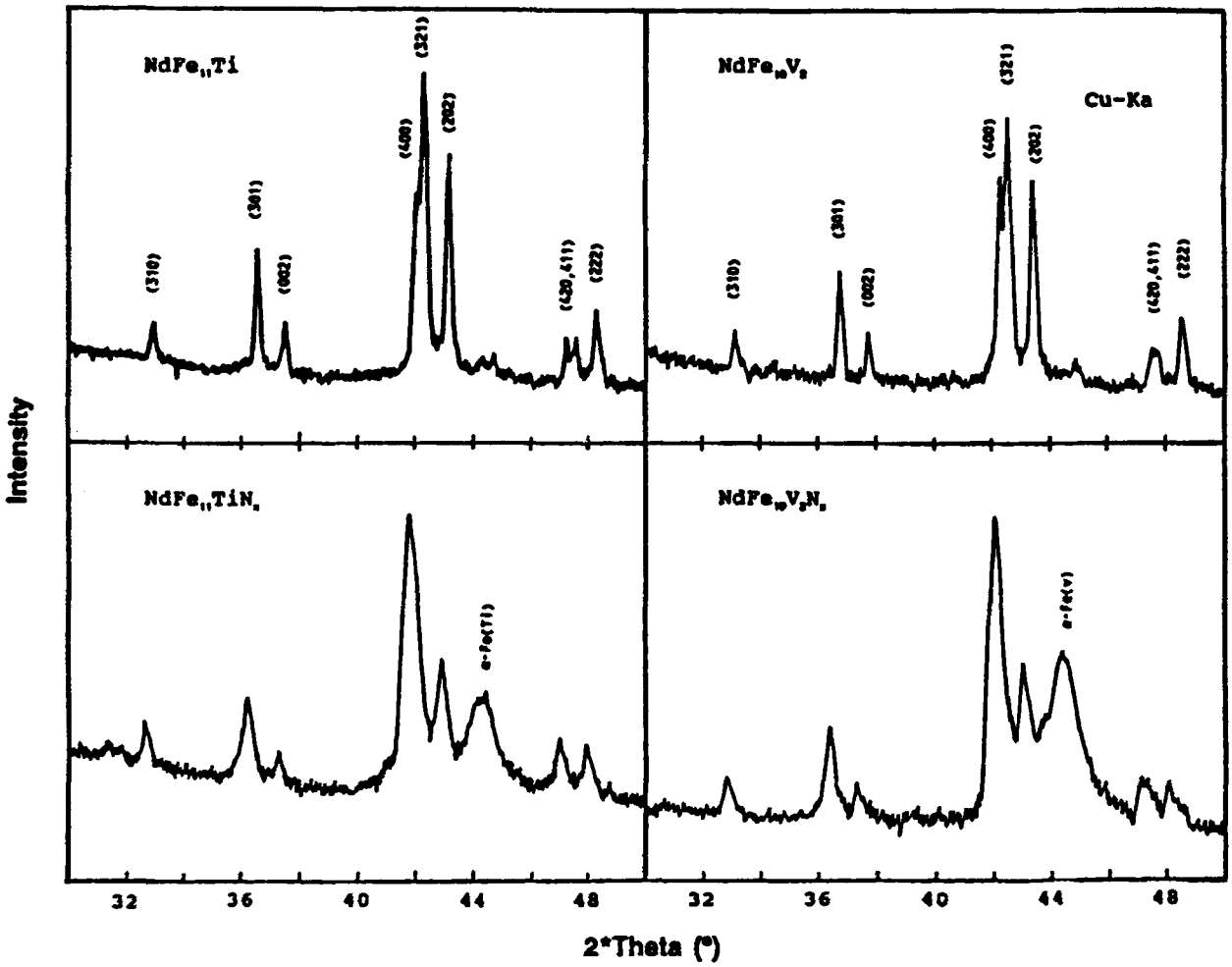

Fig. 22 Comparison of X-ray diffraction patterns for oriented $SmFe_{11}TiN_x$ and $SmFe_{10}V_2N_x$ powders with those of $SmFe_{11}Ti$ and $SmFe_{10}V_2$.

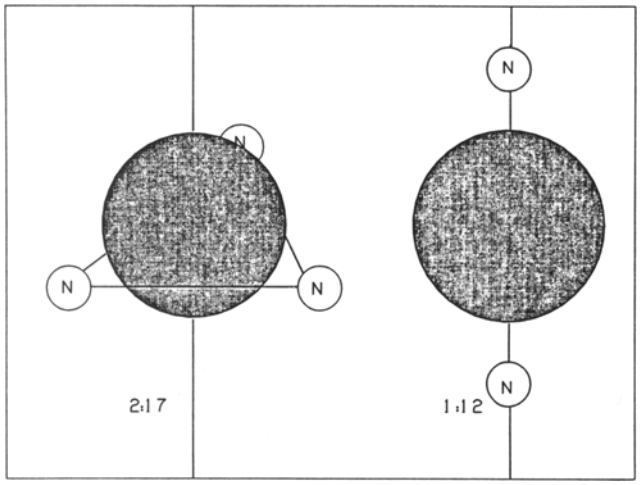

Fig. 23 Local coordination of the rare-earth atom in the interstitial compounds $R_2Fe_{17}N_x$ and $R(Fe_{12-n}M_n)N_x$.

(400) dominant. This implies that the latter nitrides exhibit a planar anisotropy.

3.4 *Effect of Nitrogenation on Electronic Properties*

The interstitial nitrogen (carbon) expands the crystal lattice modifying the Fe-Fe exchange interactions, which are about doubled, and this leads to an increase in T_c. More recently, Jaswal *et al.*[22] explained the doubling of T_c in nitrogenated 2:17 compounds nicely using self-consistent spin-polarized electronic structure calculations. Also, the nitrogen (carbon) is located around the rare-earth ions (Fig. 23), changing thus the crystal field potentials and therefore the magnetic anisotropy of the compounds.

The magnetic anisotropy of rare-earth permanent magnet materials is due to the rare-earth single ion induced anisotropy because of crystal field effects arising from the electrostatic interaction between the asymmetric charge distribution of the 4f electrons and the electrostatic field of the surrounding ions. The Hamiltonian describing this interaction is given by: [23]

$$H = \sum_{n,m} B_n^m O_n^m$$

$$B_n^m = \langle J \,||\, O \,||\, J \rangle \langle r^n \rangle A_n^m \qquad [1]$$

where $<J||O||J>$ is the Stevens factor (referred to as α_J for $n = 2$), $<r^n>$ is the Hartree-Fock radial integrals, and A_n^m is the crystal field potentials. For the rare-earth intermetallic compounds with a uniaxial-type structure, $n = 2$ is the most predominant contribution to the anisotropy (higher order terms are important in a few cases). Therefore:

$$B_2^0 = A_2^0 \alpha_J$$

$$A_2^0 = -\frac{4\pi}{5} e^2 \sum_k \frac{Z_k Y_2^0}{R_k^3} \quad [2]$$

where Y_2^0 is the spherical harmonics, Z_k is the valence number, and R_k is the distance to the kth ion. The sign and magnitude of the anisotropy constant K_1 is determined by the quantity $B = -\alpha_J (J - 1/2) A_2^0$. For Sm, α_J is positive, whereas for Nd and Pr, α_J is negative (for Gd, $\alpha_J = 0$). In Sm_2Fe_{17}, A_2^0 is also positive, and therefore, B is negative, indicating a planar anisotropy. However, in the nitrogenated compounds, the interstitial nitrogen surrounds the rare-earth ion (Fig. 23) and changes the crystal field potential A_2^0 to negative. The quantity B becomes positive, and this results in a uniaxial anisotropy. In $Nd_2Fe_{17}N_x$, because α_J is negative, the quantity B is negative, and this results in a planar anisotropy. For the $R(Fe,M)_{12}$(M = Mo, Ti, or V) compounds with the $ThMn_{12}$-type structure, the behavior is the opposite. In the nitrogen-free compounds, A_2^0 is negative, and therefore, $Sm(FeM)_{12}$ has a uniaxial anisotropy, whereas $Nd(FeM)_{12}$ has a planar anisotropy. However, after nitrogenation (Fig. 23) A_2^0 becomes negative, and now $Nd(FeM)_{12}N_x$ becomes uniaxial, whereas $Sm(FeM)_{12}N_x$ is planar.

4 Conclusions

$R_2Fe_{17}N_x$ and $RFe_{12-x}T_xN_y$ compounds have been prepared by heat-treating powders of single-phase 2:17 and 1:12 compounds in N_2 gas using the gas-phase interstitial modification process. $R_2Fe_{17}C_x$ compounds can be prepared directly from the melt with the limit of $x \sim 1.5$ and by using the gas-phase interstitial modification process with x up to 2.8. The interstitial atoms expand the crystal structure, increasing both a and c. The expansion of the unit cell volume causes significant changes in the Curie temperature (up to 300 °C) and the anisotropy field. Alloys based on $Sm_2Fe_{17}N_x(C_x)$ and $NdFe_{12-x}T_xN_y$ are the most promising for permanent magnet development because of their large uniaxial anisotropy. The maximum coercivities obtained so far are $H_c > 20$ kOe in mechanically alloyed $Sm_2Fe_{17}N_x$, $H_c = 8$ kOe in mechanically alloyed $NdFe_{10}Mo_2N_x$, $H_c = 6$ kOe in ball milled $Sm_2Fe_{17}N_x$ powders, and $H_c > 10$ kOe in Zn-bonded $Sm_2Fe_{17}N_x$ magnets.

Acknowledgments

This work was supported by DOE 90ER45413 and the U.S. Army Research Office.

References

1. D.B. de Mooij and K.H.J. Buschow, *J. Less-Common Met., 142,* 349 (1988).
2. X.P. Zhong, R.J. Radwanski, F.R. de Boer, T.H. Jacobs, and K.H.J. Buschow, *J. Magn. Magn. Mater., 86,* 333 (1990).
3. X.C. Kon, R. Grössinger, T.H. Jacobs, and K.J.H. Buschow, *J. Magn. Magn. Mater., 80,* 1 (1990).
4. J.M.D. Coey and H. Sun, *J. Magn. Magn. Mater., 87,* L251 (1990).
5. Y.Z. Wang and G.C. Hadjipanayis, *J. Appl. Phys., 70*(10), 6009 (1991).
6. J.M.D. Coey, J.F. Lawler, Hong Sun, and J.E.M. Allan, *J. Appl. Phys., 69,* 3007 (1991).
7. R.B. Helmholdt and K.H.J. Buschow, *J. Less-Common Met., 155,* 15 (1989).
8. M.W. Dirker, R.C. Thiel, L.J. de Jongh, T.H. Jacobs, and K.H.J. Buschow, *J. Less-Common Met., 155,* 339 (1989).
9. P.C.M. Gubbens, A.M. van de Kraan, T.H. Jacobs, and K.H.J. Buschow, *J. Magn. Magn. Mater., 155,* 339 (1989).
10. Y.Z. Wang and G.C. Hadjipanayis, "Magnetic Properties of $R_2Fe_{17}N_x$ Compounds" Paper No. SP1, Sixth Int. Symp. on Magnetic Anisotropy and Coercivity in Rare-Earth-Transition Metal Alloys, Pittsburgh, Oct (1990).
11. J.M.D. Coey, H. Sun, and Y. Otani, "A New Family of Rare Earth Iron Nitrides," Sixth Int. Symp. on Magnetic Anisotropy and Coercivity in Rare-Earth-Transition Metal Alloys, 36, Pittsburgh, Oct (1990).
12. K. Schnitzke, L. Schultz, J. Wecker, and M. Katter, *Appl. Phys. Lett., 57,* 2583 (1990).
13. J.M.D. Coey and H. Sun, *J. Magn. Magn. Mater., 87,* L251 (1990).
14. M.Q. Huang, L.Y. Zhang, M.M. Ma, Y. Zheng, J.M. Elbicki, W.E. Wallace, and S.G. Sankar, *J. Appl. Phys., 70*(10), 6027 (1991).
15. J.M.D. Coey in "CEAM II Annual Report," J.M.D. Coey, D. Givord, R. Harris, and R. Hanitsch, Eds. (1990).
16. K.H.J. Buschow, in *Ferromagnetic Materials,* Vol 1, E.P. Wohlfarth, Ed., North-Holland, 389 (1980).
17. U.S. Ram and P. Gaunt, *J. Appl. Phys., 54,* 2872 (1983).
18. L.X. Liao, X. Chen, Z. Altounian, and R.H. Ryan, *Appl. Phys. Lett., 60,* 129 (1992).
19. Y. Wang and G.C. Hadjipanayis, *J. Appl. Phys., 67,* 4954 (1990).
20. J.M.D. Coey, H. Sun, Y. Otani, and D.P.F. Hurley, *J. Magn. Magn. Mater., 98,* 76 (1991).
21. L. Schultz, K. Schnitzler, and J. Wecker, *J. Appl. Phys. Lett., 56,* 868 (1990).
22. S.S. Jaswal, W.B. Yelon, G.C. Hadjipanayis, Y.Z. Wang, and D.J. Sellmyer, *Phys. Rev. Lett., 67,* 644 (1991).
23. W.E. Wallace, in Rare-Earth Intermetallics, Academic Press, New York, 14 (1973).